IJMMM International Journal of Minerals, Metallurgy and Materials 矿物冶金与材料学报（英文版）

Spray pyrolysis feasibility of tungsten substitution for cobalt in nickel-rich cathode materials

Zihan Hou, Lisheng Guo, Xianlong Fu, Hongxian Zheng, Yuqing Dai, Zhixing Wang, Hui Duan, Mingxia Dong, Wenjie Peng, Guochun Yan, and Jiexi Wang

Cite this article as:
Zihan Hou, Lisheng Guo, Xianlong Fu, Hongxian Zheng, Yuqing Dai, Zhixing Wang, Hui Duan, Mingxia Dong, Wenjie Peng, Guochun Yan, and Jiexi Wang, Spray pyrolysis feasibility of tungsten substitution for cobalt in nickel-rich cathode materials, *Int. J. Miner. Metall. Mater.*, 31(2024), No. 10, pp. 2244-2252. https://doi.org/10.1007/s12613-024-2824-9

View the article online at SpringerLink or IJMMM Webpage.

INTERNATIONAL JOURNAL OF
Minerals, Metallurgy and Materials

Volume 31, Number 10, October 2024
Page 2244

Research Article https://doi.org/10.1007/s12613-024-2824-9

Spray pyrolysis feasibility of tungsten substitution for cobalt in nickel-rich cathode materials

Zihan Hou[1)], *Lisheng Guo*[1)], *Xianlong Fu*[1)], *Hongxian Zheng*[1)], *Yuqing Dai*[1)], *Zhixing Wang*[1)], *Hui Duan*[1)], *Mingxia Dong*[2)], *Wenjie Peng*[1),✉], *Guochun Yan*[1)], *and Jiexi Wang*[1),✉]

1) Key Laboratory of Value-added Metallurgy of Hunan Province, Engineering Research Center of the Ministry of Education for Advanced Battery Materials, School of Metallurgy and Environment, Central South University, Changsha 410083, China
2) BASF Shanshan Battery Materials Co. Ltd., Changsha 410205, China
(Received: 20 October 2023; revised: 27 December 2023; accepted: 2 January 2024)

Abstract: Cobalt (Co) serves as a stabilizer in the lattice structure of high-capacity nickel (Ni)-rich cathode materials. However, its high cost and toxicity still limit its development. In general, it is possible to perform transition metal substitution to reduce the Co content. However, the traditional coprecipitation method cannot satisfy the requirements of multielement coprecipitation and uniform distribution of elements due to the differences between element concentration and deposition rate. In this work, spray pyrolysis was used to prepare $LiNi_{0.9}Co_{0.1-x}W_xO_2$ (LNCW). In this regard, the pyrolysis behavior of ammonium metatungstate was analyzed, together with the substitution of W for Co. With the possibility of spray pyrolysis, the Ni–Co–W-containing oxide precursor presents a homogeneous distribution of metal elements, which is beneficial for the uniform substitution of W in the final materials. It was observed that with W substitution, the size of primary particles decreased from 338.06 to 71.76 nm, and cation disordering was as low as 3.34%. As a consequence, the prepared LNCW exhibited significantly improved electrochemical performance. Under optimal conditions, the lithium-ion battery assembled with $LiNi_{0.9}Co_{0.0925}W_{0.0075}O_2$ (LNCW-0.75mol%) had an improved capacity retention of 82.7% after 200 cycles, which provides insight into the development of Ni-rich low-Co materials. This work presents that W can compensate for the loss caused by Co deficiency to a certain extent.

Keywords: lithium-ion batteries; Ni-rich; low-cobalt; W substitution; spray pyrolysis

1. Introduction

Recently, the industry has paid increasing attention to layered cathode materials due to their advantages of comprehensive performance and low cost. In terms of battery energy density and electric vehicle driving range, ternary cathode materials containing nickel (Ni) have obvious advantages, especially in batteries with Ni-rich materials [1–4]. The demand for high-energy-density lithium (Li)-ion batteries has prompted the application and continuous improvements of high-specific-capacity Ni-rich materials [5–8]. The Ni in Ni-rich materials mostly exists as the unstable Ni^{3+} and Ni^{4+}. Because of the unpaired electron spins in the orbit, the Ni^{3+}/Ni^{4+} at the FCC octahedral position is more likely to reduce to Ni^{2+} [9]. However, Li^+ (0.076 nm) has a similar radius to Ni^{2+} (0.069 nm), resulting in Ni^{2+} migration from the 3a position of the transition metal (TM) layer to the 3b position of the Li layer. As such, Li–Ni mixing occurs, which eventuates the irreversible phase transformation of Ni-rich materials from the ideal layer structure ($R\bar{3}m$) to the spinel structure ($Fd\bar{3}m$) and finally to the rock salt structure ($Fm\bar{3}m$), significantly decreasing the rate and cycle performance of materials [10].

The inhibitory effect of cobalt (Co) on Li–Ni mixing realizes stable layer structure construction, thus improving Li-ion conductivity and significantly enhancing the electrochemical performance [11]. Thus, the improvement in performance of Ni-rich cathode materials depends on the use of expensive Co [12–13]. To overcome the challenges arising from the scarcity, high cost, and toxicity of Co, the search for low-Co and even Co-free layered oxides has been actively ongoing. Ni *et al.* [14] developed a high-performance Co-free Ni-rich Ca-pillared $LiNi_{0.845}Mn_{0.10}Al_{0.05}Ca_{0.005}O_2$ (Ca-NMA) cathode material with a layered structure coupled with fast Li^+ kinetics by activating the pinning effect with Ca^{2+} doping. The as-developed Ca-NMA cathode showed enhanced cyclability and rate capability. Park *et al.* [15] utilized a morphology engineering approach to develop a Co-free $LiNi_{0.9}Mn_{0.1}O_2$ cathode with a Ni-rich core–Mn-rich shell structure to overcome the limitations of Co-free $LiNi_xMn_{1-x}O_2$ cathodes.

Substituting an appropriate number of atoms in the crystal grain or changing the valence of certain elements is a commonly used modification technique to reduce instability problems as well as cation translocation [16]. Although coprecipitation is often selected in traditional synthesis, its

✉ Corresponding authors: Wenjie Peng E-mail: pwj_csu@163.com; Jiexi Wang E-mail: wangjiexikeen@csu.edu.cn

stringent demand for coprecipitation pH values of all included elements and the long preparation process still hinder its further application [17]. In addition, because of the separate material precipitation rate, it cannot ensure the uniform distribution of elements. Thus, it is impossible to produce a precursor material with a uniform distribution of Ni, Co, and Mn when preparing a Ni-rich material, which in turn influences the electrochemical performance of the material.

Spray pyrolysis is an effective method for preparing uniform multicomponent materials with a precise stoichiometric element ratio and uniform element distribution [18–21]. In this present work, W was selected as the substitution metal due to its dual advantages. On the one hand, the incorporated W^{6+} has a high valence state to form strong metal–oxygen bonds, which improves the stability of Ni-rich cathode materials. On the other hand, the high valence state of W^{6+} can compensate for the charge balance and regulate the degree of Li–Ni mixing to control the number of Ni^{2+} ions located in the Li slabs [22–23]. To reduce the effect of impurities and anions on the W source, ammonium metatungstate was chosen as the W source. Macroscopically, Li–Ni mixing degree and lattice parameters were determined by X-ray diffraction (XRD) and Rietveld refinement, offering strong evidence for the stability of the materials. Moreover, scanning electron microscopy (SEM), transmission electron microscopy (TEM), and energy dispersive X-ray spectroscopy (EDS) illustrated the refined particles and uniform distribution generated by spray pyrolysis. The lower degree of Li–Ni mixing and slight particles have contributed to the outstanding electrochemical performance, with a excellent capacity retention after 200 cycles and the highest reversibility. In conclusion, this study offers a possibility for the synthesis of Ni-rich low-Co cathode materials.

2. Experimental

2.1. Preparation of $LiNi_{0.9}Co_{0.1-x}W_xO_2$

Based on a molar stoichiometric ratio of $0.9:(0.1-x):x$ (x = 0.0025, 0.005, 0.0075, 0.01, 0.02, and 0.05), $NiCl_2·6H_2O$ (AR, Aladdin), $CoCl_2·6H_2O$ (AR, Aladdin), and $H_{28}N_6O_{41}W_{12}$ (AR, Aladdin) were weighed, dissolved in a certain amount of deionized water, and concentrated to a 0.5 $mol·L^{-1}$ metal salt solution to obtain the precursor solution. Then, the solution was atomized by ultrasonic atomization at a flow rate of 4 $L·min^{-1}$ of air as the current carrier gas. The atomized small droplets were placed inside a pyrolysis furnace, which was raised to the set temperature (800°C) in advance. The obtained oxide precursor $Ni_{0.9}Co_{0.1-x}W_xO_y$ was evenly mixed with $LiOH·H_2O$ (AR, Aladdin) in a mortar and pestle at a stoichiometric ratio of 1.01:1 (Li : TM). Under pure oxygen conditions, the tube furnace was heated to 500°C at 5°C·min^{-1} for presintering for 3 h and then heated at 5°C·min^{-1} to the target sintering temperature of 810°C for 15 h, finally obtaining the $LiNi_{0.9}Co_{0.1-x}W_xO_2$ (LNCW; x = 0.0025, 0.005, 0.0075, 0.01, 0.02, and 0.05) cathode materials after cooling down to room temperature.

2.2. Characterization of the materials

XRD (Empyrean 2, PANalytical, Netherlands) was used to analyze the phase structure with a Cu K_α radiation source in a sweeping step of 10°·min^{-1} over 10°–80° at 45 kV and 40 mA. The surface morphologies of the materials were characterized by field emission scanning electron microscopy (FESEM, JEOL, JSM-7900F, Japan). The morphology and microstructure of the material were analyzed by TEM (FEI, Titan G260-300, USA). The elemental valence state on the surfaces of the prepared samples was determined by X-ray photoelectron spectroscopy (XPS, EscaLab Xi+, Thermo Fisher Scientific, UK).

2.3. Electrochemical performance tests

The electrochemical performance was investigated using a 2025 coin-type half-cell. The slurry contained 80wt% active materials, 10wt% carbon black (as the conductive agent), and 10wt% polyvinylidene fluoride (as the binder) in *N*-methyl pyrrolidone. It was coated onto Al foil and dried in a vacuum oven at 90°C for 3 h. Afterward, it was cut into 12 mm-diameter disks. Li metal with a thickness of 0.5 mm and a diameter of 14 mm was utilized as counter and reference electrodes. The electrolyte comprised $LiPF_6$ (1 M) in a mixed solution of dimethyl carbonate, ethyl methyl carbonate, and ethylene carbonate (1:1:1 in volume ratio). The coin cells were assembled in an Ar-filled glove box. After standing for 12 h, the current density was set to 0.1C, 0.2C, 0.5C, 1C, 2C, and 5C (1C = 200 mA·g^{-1}), and the charge and discharge performance of the battery was measured in the voltage range of 2.8–4.3 V in a Neware battery test system. Electrochemical impedance spectroscopy (EIS) measurements were conducted using an SP-150 electrochemical workstation at 0.01–100 kHz and 5 mV. Cyclic voltammogram (CV) tests were carried out using a CHI660A electrochemical workstation at 0.1 mV·s^{-1} and 2.8–4.3 V.

3. Results and discussion

3.1. Synthesis and characterization of the precursors

To avoid interference from residual impurities, the properties of the W source must meet the requirements of exceptional solubility in water and complete decomposition at the pyrolysis temperature. Moreover, the influence of anions on the electrochemical properties of the materials should be removed to ensure that the stoichiometric ratio of each element of the prepared materials is correct. On the basis of the above considerations, ammonium metatungstate ($H_{28}N_6O_{41}W_{12}$) was elaborately selected as the W source by analysis of its pyrolysis behavior, as shown by the SEM image in Fig. 1(a), which exhibits a regular spherical morphology under the precursor preparation conditions. To examine the phase structure, the sample was investigated by XRD. Fig. 1(b) contains characteristic diffraction peaks that completely agree with the standard card of WO_3 (PDF#83-0950) and no other impurity peak, confirming that ammonium metatungstate can com-

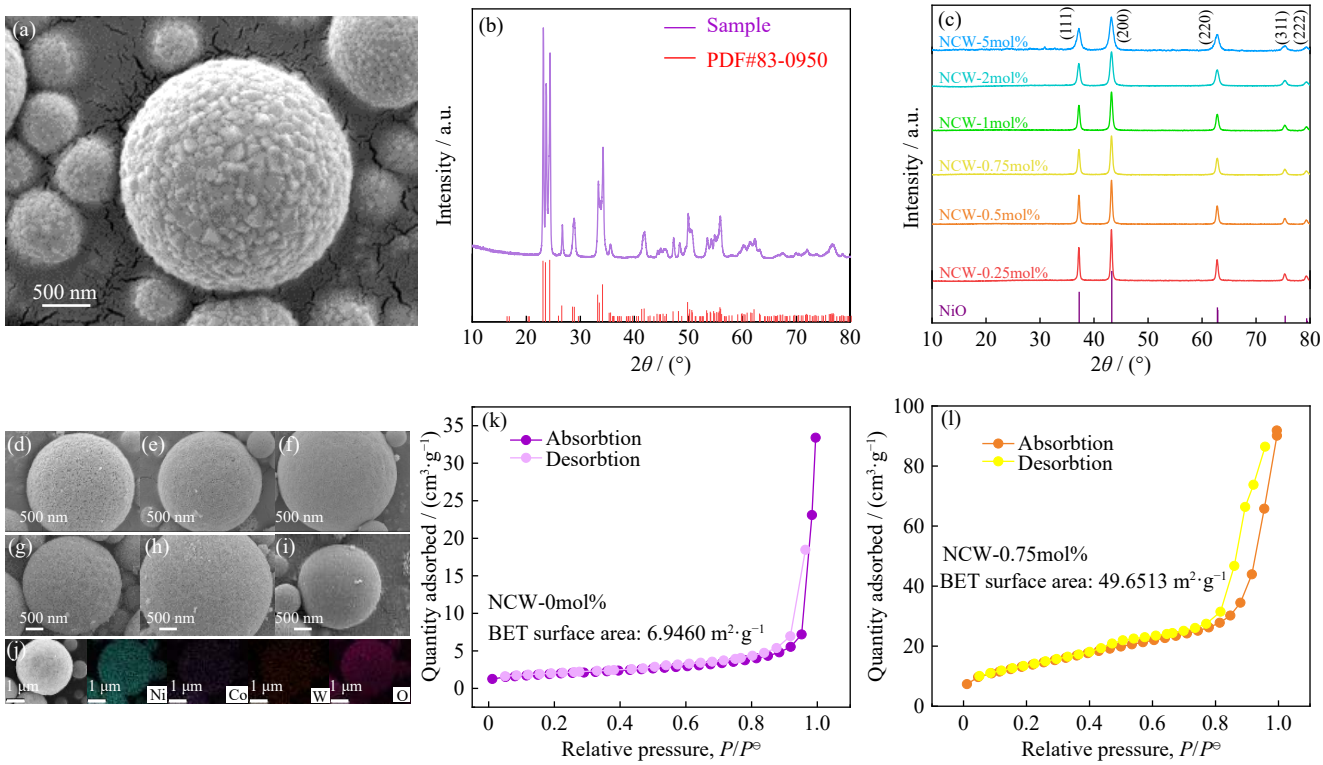

Fig. 1. (a) SEM image and (b) XRD pattern of the sample obtained by spray pyrolysis of ammonium metatungstate; (c) XRD patterns of oxide precursors with different W contents; (d–i) SEM images of (d) NCW-0.25mol%, (e) NCW-0.5mol%, (f) NCW-0.75mol%, (g) NCW-1mol%, (h) NCW-2mol%, and (i) NCW-5mol% prepared by spray pyrolysis; (j) element distribution maps of LNCW-0.25mol%; N_2 isothermal adsorption/desorption curves of (k) NCW-0mol% and (l) NCW-0.75mol%.

pletely decompose into pure phase WO_3 without introducing impurities from spray pyrolysis.

Based on the above results, $Ni_{0.9}Co_{0.1-x}W_xO_y$ (NCW) with different W contents were prepared using ammonium metatungstate as the W source. As shown in Fig. 1(c), the obtained precursor phase is consistent with standard NiO (PDF#89-7160), demonstrating that the precursor is a homogeneous solid solution structure with W substitution in the crystal. From Fig. 1(d)–(i), the precursors with different W contents all have regular spherical morphology, and the secondary spheres exhibit a porous structure with spherical particles about 0.5–3.5 μm in size. The EDS element distribution analysis results (Fig. 1(j)) exhibit that Ni, Co, W, and O in the precursor are uniformly distributed. Moreover, the Brunner–Emmet–Teller measurement (BET) results (Fig. 1(k) and (l)) indicate that the porosity increases with the W substitution.

3.2. Effect of W content on the LNCW cathode material

To examine the effect of W-substitution content on the cathode materials, a series of characterizations were applied, and the results are shown in Fig. 2. The XRD patterns in Fig. 2(a) show the diffraction peak intensity, which demonstrate that the $I_{(003)}/I_{(104)}$ ratio decreases rapidly when the W content is greater than 1mol% [24]. Moreover, LNCWs ($x \geq 1$mol%) show relatively serious Li–Ni mixing with no obvious peaks in (006)/(012) and (018)/(110) pairs, depicting that the layered structure of the materials is destroyed. Because the structure of LNCWs ($x \geq 1$mol%) is seriously inconsistent with expectations, they are no longer studied. The $I_{(003)}/I_{(104)}$ ratio is greater than 1.2 with a W content of less than 1mol%, demonstrating the slight Li–Ni mixing degree of the material [24]. Moreover, the obvious splitting of the (006)/(012) and (018)/(110) peaks shows the ideal crystallinity of the LNCWs ($x \leq 1$mol%) [25]. To further investigate the effect of W content on material lattice parameters, GSAS software was utilized to perform Rietveld full-spectrum refinement on LNCWs and show the conformity of mathematical simulation(R_w). In Fig. 2(c)–(f), with a relatively stable difference, the refined spectra are consistent with the measured spectra [26]. Also, the c value (Fig. 2(b)) of the cell parameters increase with increasing W content, demonstrating that the Li layer spacing (d) of the material increases gradually (Fig. 2(g) and (h)). On the other hand, the a value exhibits a trend of first decreasing and then increasing, primarily because when there is a small amount of substitution ($x \leq 0.5$mol%), the strong bond energy of W–O causes a shorter bond length, resulting in first decreasing of a value. With increasing W substitution amount ($x > 0.5$mol%), ionic repulsion starts to dominate, which increases the value. This gives the perfect condition for the insertion and extraction of Li ions. The Li–Ni mixing degree with different W contents can be semiquantitatively determined, which are 4.53%, 4.50%, 3.34%, and 3.85%, respectively, corresponding to LNCW-0.25mol%, LNCW-0.5mol%, LNCW-0.75mol%, LNCW-1mol%. With an increase in W content, the Li–Ni mixing degree first decreases and then increases, and the mixing degree is the lowest for LNCW-0.75mol%. This trend

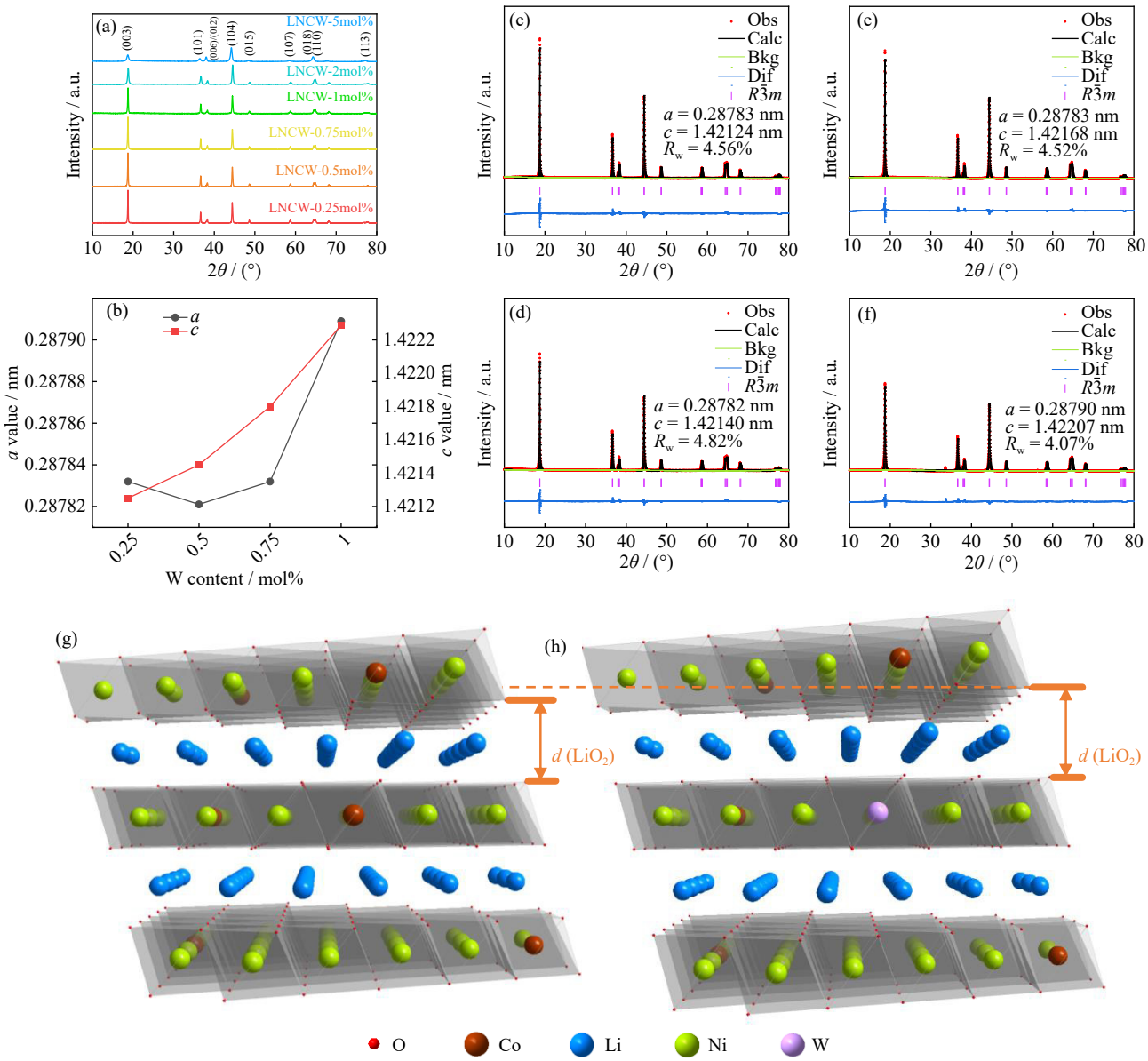

Fig. 2. (a) XRD patterns of LNCWs with different W contents; (b) *a* and *c* values of LNCWs with different W contents; Rietveld refinement results of LNCWs with different W contents: (c) 0.25mol%, (d) 0.5mol%, (e) 0.75mol%, and (f) 1.0mol%; schematic diagram of the crystal cell (g) before and (h) after substitution.

can be ascribed to two reasons. On the one hand, the inherent oxygen vacancies (V_O) produced during the synthesis result in a charge imbalance. With the W substitution ($x \leq$ 0.75mol%), the V_O content is reduced to balance the valence state, which hinders Li–Ni mixing by blocking Ni^{2+} migration. On the other hand, with further W substitution ($x \geq$ 0.75mol%), W is incorporated in $Li_xW_yO_z$ ($x/y > 1$) phases by taking Li from $LiNiO_2$, which makes it Li-deficient and has more Ni^{2+}, causing a higher degree of Li–Ni mixing [27]. A lower degree of Li–Ni mixing contributes to the acceleration of Li^+ extraction during the migration process, thereby reducing capacity loss and poor rate performance resulting from mixing [28].

Fig. 3(a)–(f) displays the SEM images of different W-substituted cathode materials. All samples with a smooth surface are formed by aggregation of multiple primary particles with different particle sizes. From Fig. 3(g), the particle size decreases with increasing W content. The smaller particle size of the material controls the internal strain, and fewer microcracks are generated inside the spheres [29–30]. On the other hand, a smaller particle size results in a shorter diffusion distance and lower solid-phase diffusion resistance, which further enhances the electrochemical properties of the materials [31–32].

In addition, TEM was conducted. Fig. 4(a) shows that the spherical morphology of the LNCW materials is damaged and exhibits an irregular polyhedral structure after sintering. From the high-resolution TEM images (Fig. 4(b)–(d)), the W-substituted materials have undergone structural evolution, and an obvious layered structure is formed on the surface of the cathode material [33]. Two different lattice stripes can be observed in the cathode material. One set of lattice stripes with a lattice spacing of 0.47 nm is assigned to the (003) crystal plane in the layered $LiNiO_2$, while the other set of lat-

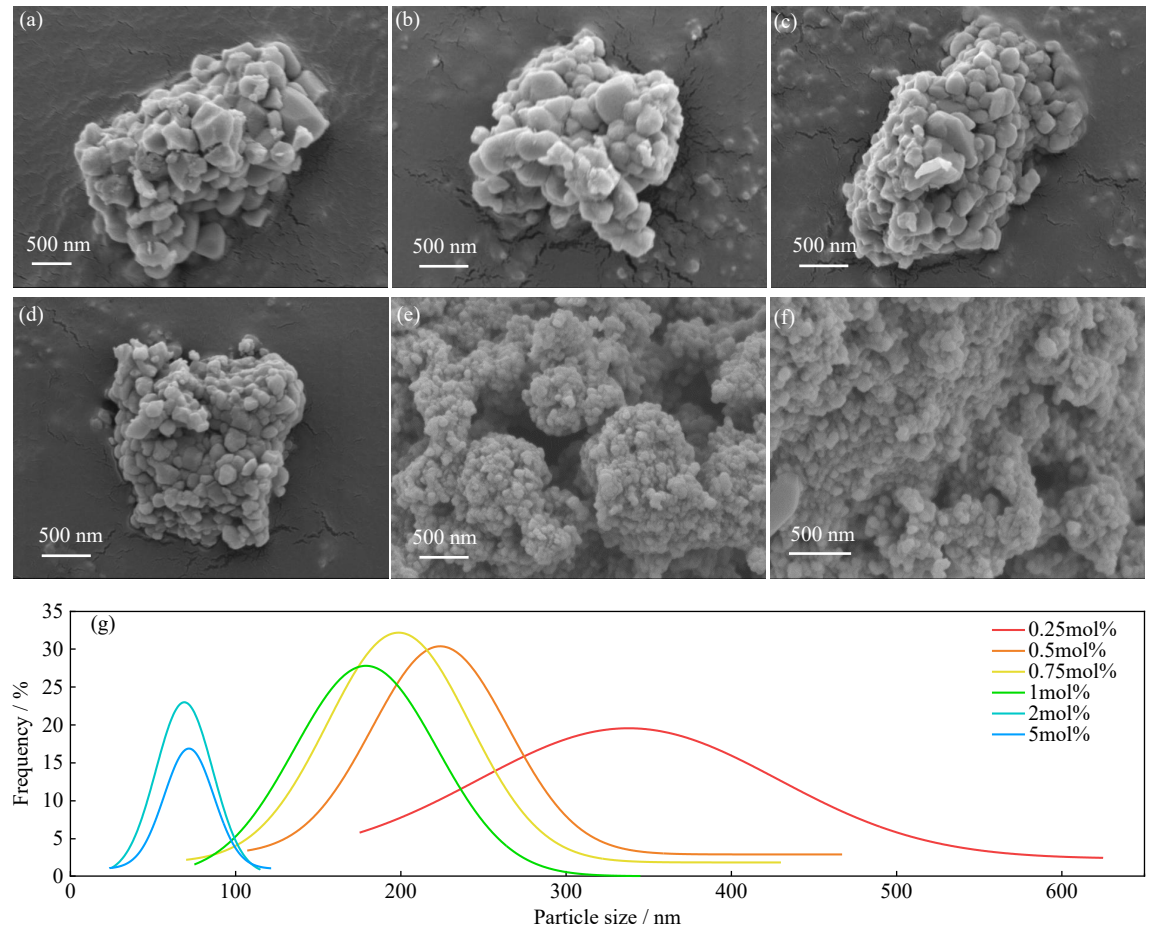

Fig. 3. SEM images of (a) LNCW-0.25mol%, (b) LNCW-0.5mol%, (c) LNCW-0.75mol%, (d) LNCW-1mol%, (e) LNCW-2mol%, and (f) LNCW-5mol%; (g) particle size fitting curves of the LNCWs.

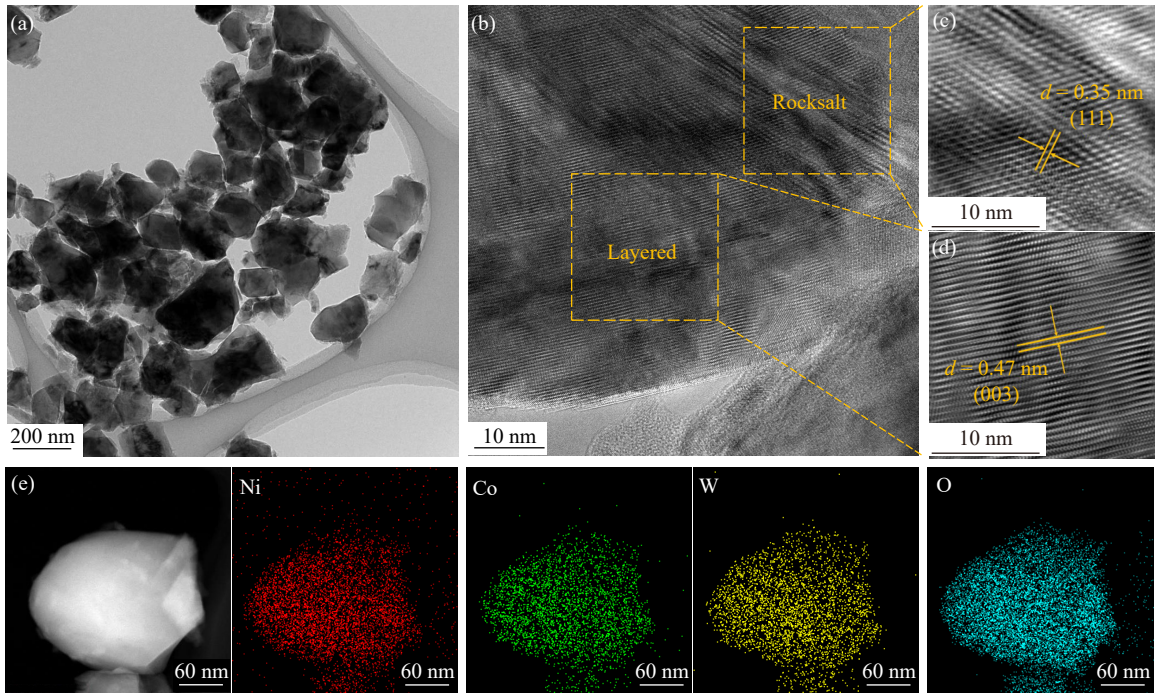

Fig. 4. (a) TEM image, (b–d) HRTEM images, and (e) EDS elemental mappings of LNCW-0.75mol%.

tice stripes with a lattice spacing of 0.35 nm is attributed to the (111) crystal plane in the rock salt phase structure Li_2WO_4 [34–35]. The latter phase is formed by partial cation mixing on the transition metal sites in the $R\bar{3}m$ lattice, which may help in capacity retention and increase the resistance of the secondary particles to microcracking under applied stress and

during charge–discharge cycling [27,36]. The evenly distributed element shown in Fig. 4(e) confirms the successful uniform replacement of W.

To examine the effect of different W-substitution contents on the electrochemical performance of LNCWs, a Li half-cell was assembled with LNCWs as the cathode material. Fig. 5(a) plots the initial charge and discharge curves of the LNCW cathode materials at 0.1C. LNCW-0.25mol%, LNCW-0.5mol%, LNCW-0.75mol%, and LNCW-1mol% have initial charge–discharge capacities of 199.2, 195.2, 193.4, and 191.7 mAh·g^{-1}, respectively. Capacity fading is associated with the electrochemical inertness of W. A higher W content results in a lower content of active elements, giving rise to a decrease in capacity. On the other hand, the cycle performance at 1C of the four samples presents similar diminution trends. In Fig. 5(b), LNCW-0.25mol%, LNCW-0.5mol%, LNCW-0.75mol%, and LNCW-1mol% deliver discharge specific capacities of 182.7, 179.9, 179.5, and 175.7 mAh·g^{-1} and maintain 52.2%, 62.8%, 82.7%, and 80.5% after 100 cycles, respectively. Compared with the sharp capacity decline of LNCWs ($x \leq 0.5$mol%), LNCWs ($x > 0.5$mol%) show superior stability. The results disclose that W substitution effectively enhances the stability of Ni-rich cathode materials, with LNCW-0.75mol% recording the best electrochemical performance. As shown in Fig. 5(c)–(f), when the current changes from 1C to 5C, the specific capacity attenuation of LNCWs are 39.3, 25.2, 17.4, and 47.4 mAh·g^{-1}, respectively, corresponding to LNCW-0.25mol%, LNCW-0.5mol%, LNCW-0.75mol%, and LNCW-1mol%. According to the XRD pattern (Fig. 2(a)), LNCW-0.75mol% displays the lowest degree of Li–Ni mixing, helping to improve the capacity, as well as stability. In addition, the smaller primary particle size of LNCW-0.75mol% in Fig. 3 also contributes to a shorter Li^+ transmission path, thus boosting

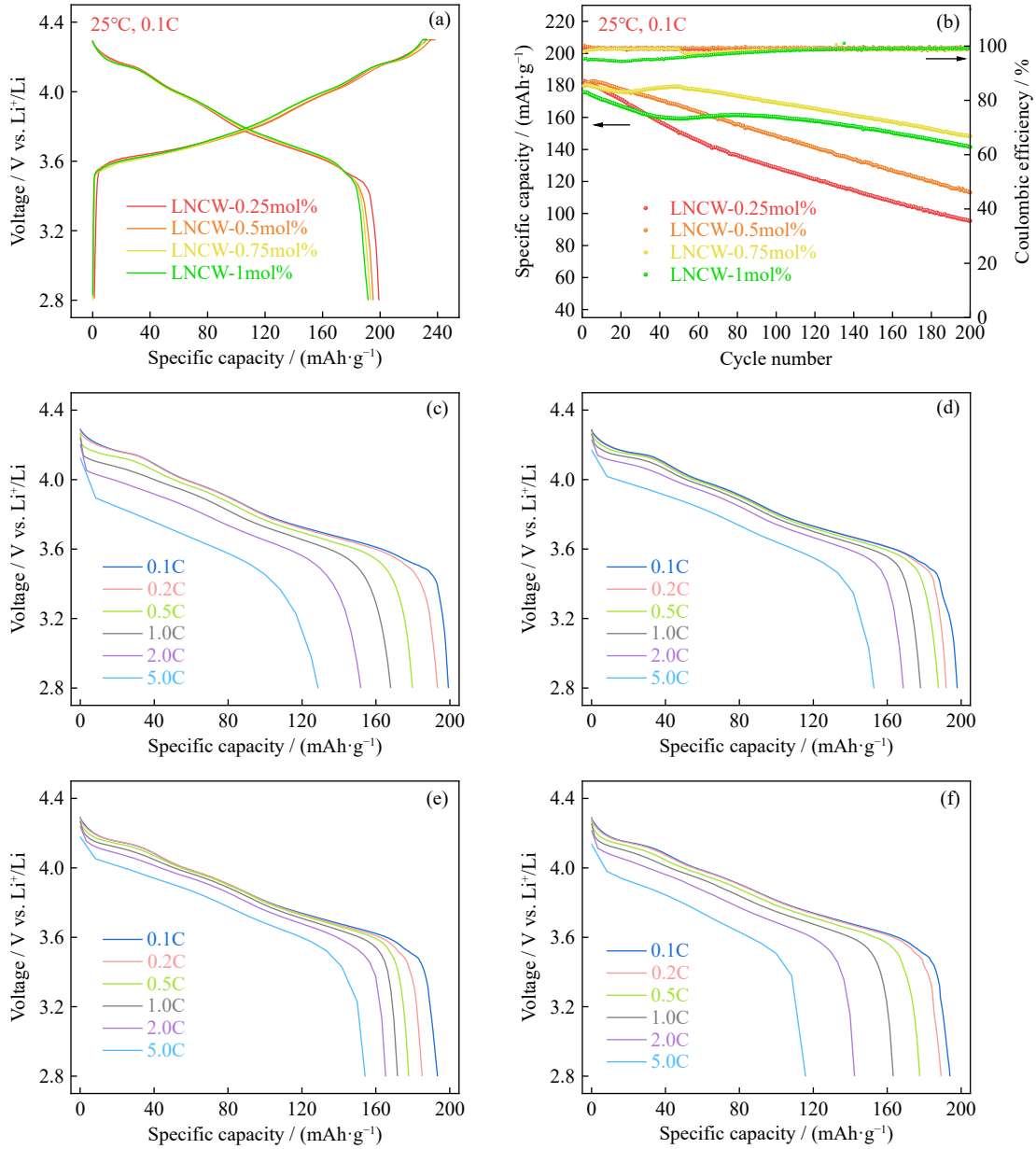

Fig. 5. (a) Initial charge and discharge curves at 0.1C for LNCWs; (b) cycling performance at 1C under 25°C; discharge curves at different rates for (c) LNCW-0.25mol%, (d) LNCW-0.5mol%, (e) LNCW-0.75mol%, and (f) LNCW-1.0mol%.

its rate performance [37].

3.3. Mechanism for the improvement of performance in the LNCWs

To further prove the possibility and mechanism of W substitution, a series of experiments were conducted. First, XPS was conducted, and the C 1s peak (284.80 eV) was used for the normalization of all the spectra. The W 4f spectrum of LNCW-0.75mol% displays two characteristic peaks at 35.33 and 37.48 eV (Fig. 6(a)), which are attributed to W^{6+} in Li_2WO_4, demonstrating the successful W substitution in LNCW cathode materials [38]. Fig. 6(b) shows the Ni 2p spectra of LNCWs. In general, the characteristic peak (855.0 eV) of the Ni $2p_{3/2}$ spectrum is assigned to the coinciding result of Ni^{2+} and Ni^{3+}, and the decrease in Ni^{3+} content shows as the peak movement to higher binding energy [39–40]. With increasing W content, the shift of the peaks demonstrates that the Ni^{3+} content first decreases and then increases, which is ascribed to twofold reasons. First, when the W content is less than 0.5mol%, part of Ni^{3+} is reduced to Ni^{2+} to balance the valence state due to the high valence state of W^{6+}, which increases Ni^{2+} content [41]. With the further increase in W content, the LNCW particles (x > 0.5mol%) are obviously refined with a greater specific surface area, which is more conducive to contact with LiOH [42]. This is also favorable for the conversion of Ni^{2+} to Ni^{3+} in the precursor so that the Ni^{3+} content gradually increases.

Furthermore, CV was conducted to confirm the polarization and reversibility of the LNCWs in the potential range of 2.8–4.3 V. In Fig. 6(c)–(f), the three redox peaks for low to high potential are associated with the phase transitions of H1 to M, M to H2, and H2 to H3, respectively [43–44]. In general, the potential differences (ΔE_P) between the redox peaks in the CV curve can be utilized as a criterion for assessing the polarization of materials. A smaller ΔE_P is conducive to polarization reduction and reversibility construction of materials [45–46]. With increasing W-substitution amount, ΔE_P first decreases and then increases. LNCW-0.75mol%, with the smallest ΔE_P, displays the highest reversibility and minimal polarization degree, probably due to its low Li–Ni mixing degree, which speeds up the migration rate of Li^+. EIS tests were performed to further explore the evolution of electrochemical resistance and kinetic behavior before the initial cycle and after 200 cycles at 1C (Fig. 6(g) and (h)) [47]. In general, an x-axis intercept and two semicircles of fitting curves at different charging states correspond to Ohmic res-

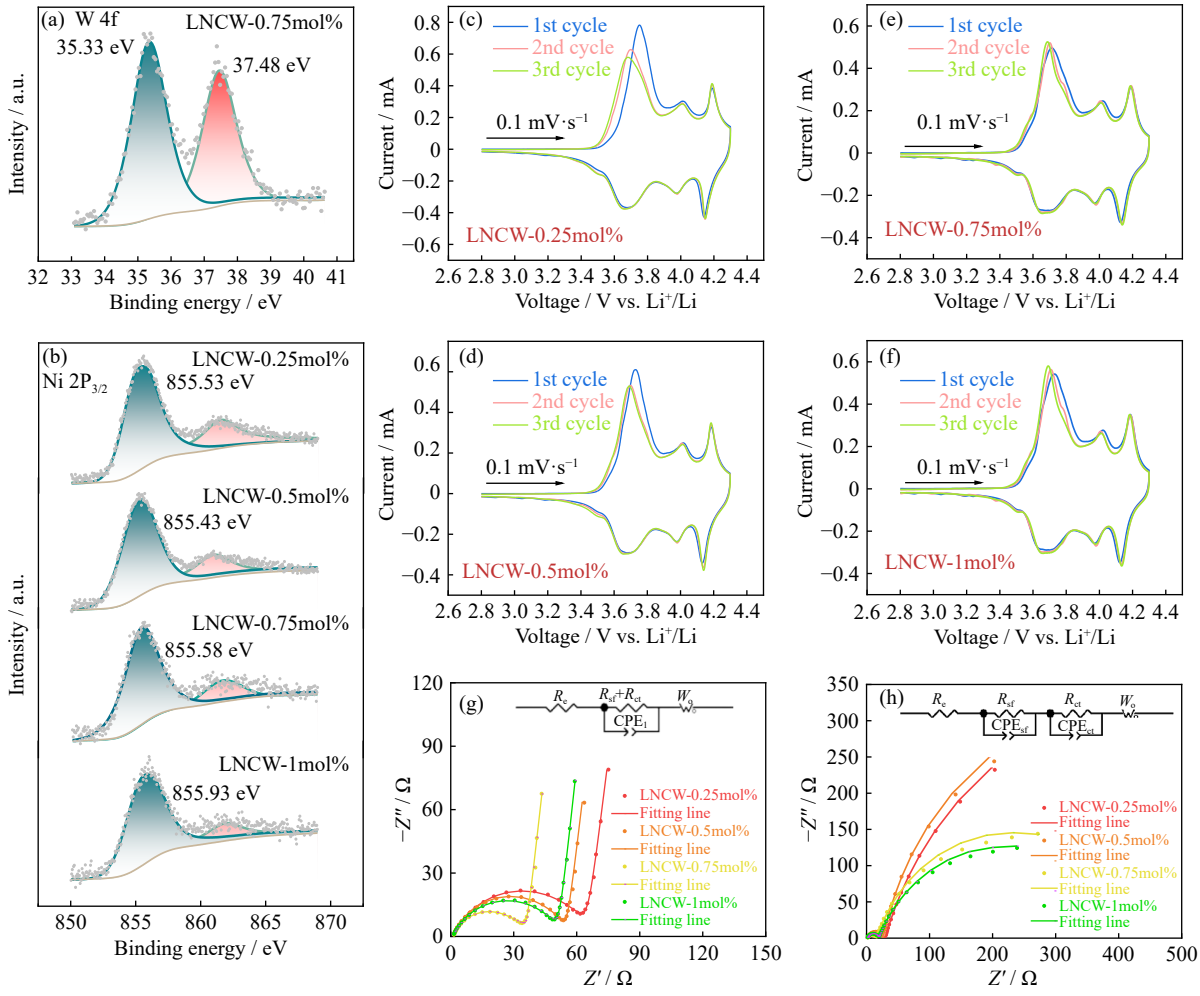

Fig. 6. (a) XPS spectra of W 4f for LNCW-0.75mol%; (b) XPS spectra of Ni $2p_{3/2}$ for LNCWs; CV curves of LNCWs (c) 0.25mol%, (d) 0.5mol%, (e) 0.75mol%, and (f) 1mol%; EIS Nyquist diagrams and fitting curves for LNCWs (g) before and (h) after 200 cycles at 1C.

istance (R_e), solid electrolyte interphase film resistance (R_{sf}) at high frequency, and charge transfer resistance (R_{ct}) at medium frequency, respectively [48–49]. Fig. 6(g) exhibits similar impedance values of the LNCWs before the initial cycle. In contrast, the cycled impedance values show intensive differences. LNCW-0.75mol% has the smallest R_{sf} and R_{ct} of 13.74 and 355.8 Ω, respectively, indicating that an appropriate amount of W substitution can decrease the charge transfer impedance and improve the charge–discharge reversibility. In the equivalent circuit, CPE represents the constant phase angle element associated with the double-layer capacitor, and W_o represents the solid-state diffusion impedance. However, excessive W-substitution results in slow kinetic behavior and irreversibility during cycling. The moderate W substitution allows a stable layered structure, which contributes to a low degree of Li–Ni mixing and fast Li^+ migration.`

4. Conclusion

Due to the high cost and toxicity of Co, W-substituted cathode materials were prepared by spray pyrolysis with ammonium metatungstate as the W source because of its good solubility and complete decomposition at the pyrolysis temperature without introducing impurity anions. It was shown that W is successfully substituted into the oxide precursor with uniform distribution. The prepared materials with W substitution demonstrated refined primary particles and a reduced degree of Li–Ni mixing. As a consequence, the Li^+ transmission path was shortened, and the cycle stability of Ni-rich materials was enhanced. At a W-substitution amount of 0.75mol%, the obtained LNCW-0.75mol% cathode has the best performance and capacity retention. This work provides a possible strategy for the synthesis of Ni-rich low-Co materials with various substitutions.

Acknowledgements

This work was financially supported by the National Natural Science Foundation of China (No. 52122407), the Science and Technology Innovation Program of Hunan Province, China (No. 2022RC3048), and the Key Research and Development Program of Yunnan Province, China (No. 202103AA080019).

Conflict of Interest

All authors declare that there are no competing interests.

References

[1] B. Dunn, H. Kamath, and J.M. Tarascon, Electrical energy storage for the grid: A battery of choices, *Science*, 334(2011), No. 6058, p. 928.

[2] W. Li, A. Sasaki, H. Oozu, *et al*., Electron transport mechanism of tungsten trioxide powder thin film studied by investigating effect of annealing on resistivity, *Microelectron. Reliab.*, 55(2015), No. 2, p. 407.

[3] N. Nitta, F.X. Wu, J.T. Lee, and G. Yushin, Li-ion battery materials: Present and future, *Mater. Today*, 18(2015), No. 5, p. 252.

[4] J.J. Xu, T.P. Pollard, C.Y. Yang, *et al*., Lithium halide cathodes for Li metal batteries, *Joule*, 7(2023), No. 1, p. 83.

[5] L. Yu, T.C. Liu, R. Amine, J.G. Wen, J. Lu, and K. Amine, High nickel and No cobalt─The pursuit of next-generation layered oxide cathodes, *ACS Appl. Mater. Interfaces*, 14(2022), No. 20, p. 23056.

[6] J.M. Zheng, M. Gu, A. Genc, *et al*., Mitigating voltage fade in cathode materials by improving the atomic level uniformity of elemental distribution, *Nano Lett.*, 14(2014), No. 5, p. 2628.

[7] L.F. Wang, J.Y. Wang, L.Y. Wang, M.J. Zhang, R. Wang, and C. Zhan, A critical review on nickel-based cathodes in rechargeable batteries, *Int. J. Miner. Metall. Mater.*, 29(2022), No. 5, p. 925.

[8] A. Iqbal, L. Chen, Y. Chen, Y.X. Gao, F. Chen, and D.C. Li, Lithium-ion full cell with high energy density using nickel-rich $LiNi_{0.8}Co_{0.1}Mn_{0.1}O_2$ cathode and SiO–C composite anode, *Int. J. Miner. Metall. Mater.*, 25(2018), No. 12, p. 1473.

[9] J. Zhu, S. Sharifi-Asl, J.C. Garcia, *et al*., Atomic-level understanding of surface reconstruction based on $Li[Ni_xMn_yCo_{1-x-y}]O_2$ single-crystal studies, *ACS Appl. Energy Mater.*, 3(2020), No. 5, p. 4799.

[10] D. Streich, C. Erk, A. Guéguen, P. Müller, F.F. Chesneau, and E.J. Berg, *Operando* monitoring of early Ni-mediated surface reconstruction in layered lithiated Ni–Co–Mn oxides, *J. Phys. Chem. C*, 121(2017), No. 25, p. 13481.

[11] T.C. Liu, L. Yu, J.J. Liu, *et al*., Understanding Co roles towards developing Co-free Ni-rich cathodes for rechargeable batteries, *Nat. Energy*, 6(2021), p. 277.

[12] K. Kang, Y.S. Meng, J. Bréger, C.P. Grey, and G. Ceder, Electrodes with high power and high capacity for rechargeable lithium batteries, *Science*, 311(2006), No. 5763, p. 977.

[13] W.M. Seong, K. Yoon, M.H. Lee, S.K. Jung, and K. Kang, Unveiling the intrinsic cycle reversibility of a $LiCoO_2$ electrode at 4.8-V cutoff voltage through subtractive surface modification for lithium-ion batteries, *Nano Lett.*, 19(2019), No. 1, p. 29.

[14] L.S. Ni, H.Y. Chen, J.Q. Gao, *et al*., Calcium-induced pinning effect for high-performance Co-free Ni-rich NMA layered cathode, *Nano Energy*, 115(2023), art. No. 108743.

[15] G.T. Park, H.H. Sun, T.C. Noh, *et al*., Nanostructured Co-free layered oxide cathode that affords fast-charging lithium-ion batteries for electric vehicles, *Adv. Energy Mater.*, 12(2022), No. 48, art. No. 2202719.

[16] M. Chen, W.L. Ao, C.S. Dai, T. Tao, and J. Yang, Synthesis and electrochemical properties of $LiNi_{0.8}Al_{0.2-x}Ti_xO_2$ cathode materials by an ultrasonic-assisted co-precipitation method, *Int. J. Miner. Metall. Mater.*, 16(2009), No. 4, p. 452.

[17] Y. Xia, J.M. Zheng, C.M. Wang, and M. Gu, Designing principle for Ni-rich cathode materials with high energy density for practical applications, *Nano Energy*, 49(2018), p. 434.

[18] L.H. Liu, M.C. Li, L.H. Chu, *et al*., Layered ternary metal oxides: Performance degradation mechanisms as cathodes, and design strategies for high-performance batteries, *Prog. Mater. Sci.*, 111(2020), art. No. 100655.

[19] J. Leng, J.P. Wang, W.J. Peng, *et al*., Highly-dispersed submicrometer single-crystal nickel-rich layered cathode: Spray synthesis and accelerated lithium-ion transport, *Small*, 17(2021), No. 14, art. No. 2006869.

[20] Y. Li, X.H. Li, Z.X. Wang, H.J. Guo, and J.X. Wang, Spray pyrolysis synthesis of nickel-rich layered cathodes $LiNi_{1-2x}Co_xMn_xO_2$ (x=0.075, 0.05, 0.025) for lithium-ion batteries, *J. Energy Chem.*, 27(2018), No. 2, p. 447.

[21] T. Li, X.H. Li, Z.X. Wang, and H.J. Guo, A short process for the efficient utilization of transition-metal chlorides in lithium-ion batteries: A case of $Ni_{0.8}Co_{0.1}Mn_{0.1}O_{1.1}$ and $LiNi_{0.8}Co_{0.1}$-

$Mn_{0.1}O_2$, *J. Power Sources*, 342(2017), p. 495.
[22] K.B. Fang, Q. Xie, C.Y. Wang, *et al*., Understanding the feasibility of manganese substitution for cobalt in the synthesis of nickel-rich and cobalt-free cathode materials, *ACS Appl. Energy Mater.*, 4(2021), No. 7, p. 7190.
[23] Y. Cho, P. Oh, and J. Cho, A new type of protective surface layer for high-capacity Ni-based cathode materials: Nanoscaled surface pillaring layer, *Nano Lett.*, 13(2013), No. 3, p. 1145.
[24] T. Ohzuku, A. Ueda, and M. Nagayama, Electrochemistry and structural chemistry of $LiNiO_2$ ($R\bar{3}m$) for 4 volt secondary lithium cells, *J. Electrochem. Soc.*, 140(1993), No. 7, p. 1862.
[25] Y. Gao, M.V. Yakovleva, and W.B. Ebner, Novel $LiNi_{1-x}Ti_{x/2}Mg_{x/2}O_2$ compounds as cathode materials for safer lithium-ion batteries, *Electrochem. Solid-State Lett.*, 1(1999), No. 3, art. No. 117.
[26] P. Fu, Y.M. Zhao, Y.Z. Dong, X.N. An, and G.P. Shen, Low temperature solid-state synthesis routine and mechanism for $Li_3V_2(PO_4)_3$ using LiF as lithium precursor, *Electrochim. Acta*, 52(2006), No. 3, p. 1003.
[27] C.X. Geng, D. Rathore, D. Heino, *et al*., Mechanism of action of the tungsten dopant in $LiNiO_2$ positive electrode materials, *Adv. Energy Mater.*, 12(2022), No. 6, art. No. 2103067.
[28] K. Kang and G. Ceder, Factors that affect Li mobility in layered lithium transition metal oxides, *Phys. Rev. B*, 74(2006), No. 9, art. No. 094105.
[29] D.W. Wang, C.B. Zhu, Y.P. Fu, X.L. Sun, and Y. Yang, Interfaces in garnet-based all-solid-state lithium batteries, *Adv. Energy Mater.*, 10(2020), No. 39, art. No. 2001318.
[30] Y.Y. Sun, P.Y. Hou, and L.C. Zhang, Mitigating the microcracks of high-Ni oxides by *in situ* formation of binder between anisotropic grains for lithium-ion batteries, *ACS Appl. Mater. Interfaces*, 12(2020), No. 12, p. 13923.
[31] J.H. Park, K. Park, D. Han, *et al*., Structure- and porosity-tunable, thermally reactive metal organic frameworks for high-performance Ni-rich layered oxide cathode materials with multiscale pores, *J. Mater. Chem. A*, 7(2019), No. 25, p. 15190.
[32] X.X. Zhao, B.S. Liu, J.L. Yang, J.J. Hou, Y.X. Wang, and Y.L. Zhu, Synthesizing $LiNi_{0.5}Co_{0.2}Mn_{0.3}O_2$ with microsized peanut-like structure for enhanced electrochemical properties of lithium ion batteries, *J. Alloys Compd.*, 832(2020), art. No. 154464.
[33] Z. Gan, G. Hu, Z. Peng, Y. Cao, H. Tong, and K. Du, Surface modification of $LiNi_{0.8}Co_{0.1}Mn_{0.1}O_2$ by WO_3 as a cathode material for LIB, *Appl. Surf. Sci*., 481(2019), p. 1228.
[34] S. Lee, J. Hwang, C. Park, S. Ahn, and H. Ahn, Efficient and scalable encapsulation process of highly conductive 1T-MoS_2 nanosheets on Ni-rich $LiNi_{0.83}Co_{0.11}Mn_{0.06}O_2$ cathode materials for high-performance lithium-ion batteries, *Chem. Eng. J.*, 470(2023), art. No. 144209.
[35] H.L. Zhang, F. Omenya, P.F. Yan, *et al*., Rock-salt growth-induced (003) cracking in a layered positive electrode for Li-ion batteries, *ACS Energy Lett.*, 2(2017), No. 11, p. 2607.
[36] U.H. Kim, D.W. Jun, K.J. Park, *et al*., Pushing the limit of layered transition metal oxide cathodes for high-energy density rechargeable Li ion batteries, *Energy Environ. Sci.*, 11(2018), No. 5, p. 1271.
[37] T. He, Y. Lu, Y.F. Su, *et al*., Sufficient utilization of zirconium ions to improve the structure and surface properties of nickel-rich cathode materials for lithium-ion batteries, *ChemSusChem*, 11(2018), No. 10, p. 1639.
[38] T.T. Dao, S. Park, S. Sarwar, *et al*., Novel flexible photochromic device with unprecedented fast-bleaching kinetic via platinum decoration on WO_3 layer, *Sol. Energy Mater. Sol. Cells*, 231(2021), art. No. 111316.
[39] S.Y. Peng, X.B. Kong, J.Y. Li, J. Zeng, and J.B. Zhao, Alleviating the storage instability of $LiNi_{0.8}Co_{0.1}Mn_{0.1}O_2$ cathode materials by surface modification with poly(acrylic acid), *ACS Sustainable Chem. Eng.*, 9(2021), No. 22, p. 7466.
[40] B.Z. You, J.P. Sun, Y. Jing, *et al*., A fresh one-step spray pyrolysis approach to prepare nickel-rich cathode material for lithium-ion batteries, *ACS Appl. Mater. Interfaces*, 15(2023), No. 11, p. 14587.
[41] S. Gao, X.W. Zhan, and Y.T. Cheng, Structural, electrochemical and Li-ion transport properties of Zr-modified $LiNi_{0.8}Co_{0.1}Mn_{0.1}O_2$ positive electrode materials for Li-ion batteries, *J. Power Sources*, 410-411(2019), p. 45.
[42] H.H. Ryu, K.J. Park, D.R. Yoon, A. Aishova, C.S. Yoon, and Y.K. Sun, $Li[Ni_{0.9}Co_{0.09}W_{0.01}]O_2$: A new type of layered oxide cathode with high cycling stability, *Adv. Energy Mater.*, 9(2019), No. 44, art. No. 1902698.
[43] H.H. Ryu, G.T. Park, C.S. Yoon, and Y.K. Sun, Suppressing detrimental phase transitions *via* tungsten doping of $LiNiO_2$ cathode for next-generation lithium-ion batteries, *J. Mater. Chem. A*, 7(2019), No. 31, p. 18580.
[44] F. Wu, N. Liu, L. Chen, *et al*., Improving the reversibility of the H2-H3 phase transitions for layered Ni-rich oxide cathode towards retarded structural transition and enhanced cycle stability, *Nano Energy*, 59(2019), p. 50.
[45] Z.Y. Zhang, S. Zhang, S.X. Geng, S.B. Zhou, Z.L. Hu, and J.Y. Luo, Agglomeration-free composite solid electrolyte and enhanced cathode-electrolyte interphase kinetics for all-solid-state lithium metal batteries, *Energy Storage Mater.*, 51(2022), p. 19.
[46] Q. Sun, G.F. Zeng, J. Li, *et al*., Is soft carbon a more suitable match for SiO_x in Li-ion battery anodes? *Small*, 19(2023), No. 37, art. No. e2302644.
[47] L.F. Wang, M.M. Geng, X.N. Ding, *et al*., Research progress of the electrochemical impedance technique applied to the high-capacity lithium-ion battery, *Int. J. Miner. Metall. Mater.*, 28(2021), No. 4, p. 538.
[48] P.Y. Hou, J.M. Yin, M. Ding, J.Z. Huang, and X.J. Xu, Surface/interfacial structure and chemistry of high-energy nickel-rich layered oxide cathodes: Advances and perspectives, *Small*, 13(2017), No. 45, art. No.1701802.
[49] M. Weiss, R. Ruess, J. Kasnatscheew, *et al*., Fast charging of lithium-ion batteries: A review of materials aspects, *Adv. Energy Mater.*, 11(2021), No. 33, art. No. 2101126.